RSC Advances

PAPER

View Article Online
View Journal | View Issue

Cite this: *RSC Adv.*, 2026, **16**, 13612

Context-dependent cytotoxicity and ADMET profiling of methoxylated flavonoids as novel leads for metastatic prostate cancer

Wafa Hourani *

Prostate cancer continues to be a leading cause of cancer-related mortality among men. Acquired resistance to currently available treatment options necessitates discovery of novel bioactive scaffolds. Flavonoids, a group of plant-derived polyphenolic compounds, have been shown to interfere with cellular mechanisms such as mitochondrial functioning, cell-cycle progression and apoptotic cell death. The current study assessed the cytotoxic activity, cellular uptake and apoptosis-inducing properties of six structurally diverse methoxylated flavonoids isolated from Varthemia iphionoides, namely jaceidin (V1), kumatakenin (V2), 4′-hydroxy-3,5,6,7-tetramethoxyflavone (V3), santin (V4), quercetin-3,3′-dimethyl ether (V5) and 6-methoxyisokaempferide (V6) in metastatic prostate cancer cell lines PC3 and DU145. The cytotoxic activity of these compounds was assessed using MTT assay and the apoptosis, mitochondrial membrane potential and cell-cycle phases were analyzed employing flow cytometry-based assays. Flavonoids V3, V5 and V6 demonstrated the most promising cytotoxic activities among the series. Compound V3 exhibited IC50 values of 7.22 ± 0.21 μM and 1.30 ± 0.69 μM, V5 of 5.16 ± 0.13 μM and 28.17 ± 2.74 μM, while V6 showed 1.67 ± 0.87 μM and 1.90 ± 0.88 μM in PC3 and DU145 cell lines respectively. Flavonoid V3 mediated perturbation of cell-cycle dynamics was cell line specific *via* G2/M phase arrest in PC3 cells (45.2 ± 2.0% at 48 h along with significant sub-G1 population *i.e.* 8.9 ± 0.7%) and S-phase accumulation in DU145 cells (40.1 ± 1.9% at 48 h with sub-G1 population of 6.3 ± 0.5%). A moderate rate of apoptosis and significant MMP depolarization was observed, indicating the role of mitochondria-associated cell death pathways. The *in silico* ADMET profile of the compounds revealed good drug-likeness properties hence pointing to the lead like nature of these compounds. The overall data signify the potential of methoxylated flavonoids as modulators of mitochondrial functioning and cell-cycle dynamics in metastatic prostate cancer.

Received 28th November 2025
Accepted 2nd March 2026

DOI: 10.1039/d5ra09216g

rsc.li/rsc-advances

1. Introduction

Prostate cancer is the most common cancer in men globally, with metastatic stages largely unresponsive to standard therapies including chemotherapy.[1] This reality underlines an urgent unmet need for the development of novel cancer-selective killing agents with minimum side effects.[2] In this context, natural products including flavonoids are highly valued due to their broad spectrum of bioactivities, with reports of antineoplastic, antioxidant, and anti-inflammatory properties.[3] Flavonoids are a cluster of polyphenolic molecules regularly present in fruits, vegetables, and medicinal plants. The demonstrated role of flavonoids in the regulation of several critical intracellular signaling pathways involved in cancer promotion has made them potential hits for new drug discovery.[4] Several recent studies have reported that flavonoids can sensitize cancer cells to certain chemotherapeutic agents and even potentiate the efficacy of established anti-cancer drugs by twofold.[5,6]

Mitochondria play a central role in the decision-making events of cell fate between survival and apoptosis, and thus, have been a central consideration in several cancer therapeutic strategies.[7] Mitochondrial membrane depolarization is the primary event in the intrinsic apoptosis pathway, leading to the release of cytochrome C, activation of caspases, and eventual apoptosis.[8] Likewise, recently reported synthetic tetramethoxy flavones have been reported to increase ROS, selectively impair mitochondria, and induce apoptosis.[9,10] For example, the natural phytochemical compound quercetin and its conjugates were reported to cause MMP depolarization and down-regulation of caspase-3 proteins as a principal reason for their observed anticancer effects in prostate cancer cells.[11] On the other hand, some semisynthetic analogs of flavonoids, tetramethoxy flavones have been shown to selectively induce mitochondrial impairment, ROS generation, and apoptosis.[12]

Despite the well-accepted anticancer efficacy of flavonoids, their mechanism of action, and level of efficacy in different

Department of Pharmaceutical Sciences, Faculty of Pharmacy, Philadelphia University, P. O. Box 1, Amman, 19392, Jordan. E-mail: whourani@philadelphia.edu.jo

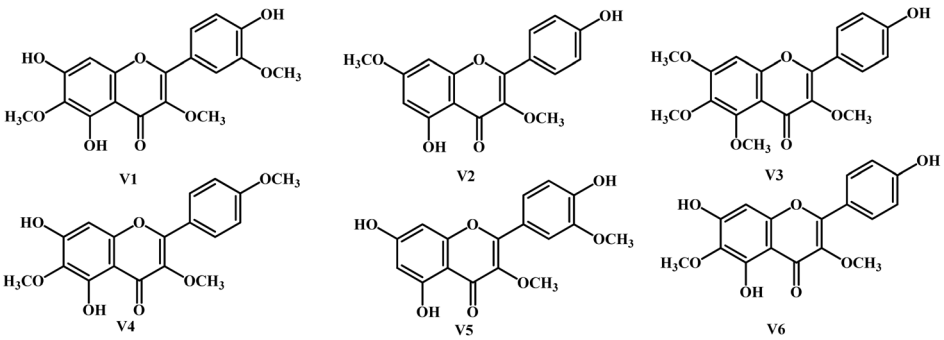

Fig. 1 Jaceidin (V1), kumatakenin (V2), 4′-hydroxy-3,5,6,7-tetramethoxyflavone (V3), santin (V4), quercetin-3,3′-dimethyl ether (V5) and viscosine (V6).

prostate cancer models are still not understood. Tumor heterogeneity particularly between the bone and brain metastasis-derived cell lines profoundly influences their response to drug treatment and sensitivity.[13] PC3, of bone origin, exhibits higher basal ROS levels and higher sensitivity to mitochondrial-targeting drugs compared to DU145 cells of brain origin.[14] These differences emphasize the significance of evaluating candidate anticancer compounds through several prostate cancer models to better recognize cell line–specific responses.

In this study, we performed a systematic pharmacological evaluation of six flavonoids isolated from *Varthemia iphionoides*: jaceidin (V1), kumatakenin (V2), 4′-hydroxy-3,5,6,7-tetramethoxyflavone (V3), santin (V4), quercetin-3,3′-dimethyl ether (V5), and viscosine (V6) (Fig. 1). Their anticancer activity was assessed in two metastatic prostate cancer cell lines, PC3 and DU145, using MTT cytotoxicity assays, mitochondrial membrane potential analysis, and Annexin V-FITC/propidium iodide apoptosis assays.

Simultaneously, *in silico* ADMET (absorption, distribution, metabolism and excretion and toxicity) profiling was used as a preliminary measure to rank lead-like compounds based on anticipated drug-likeness, pharmacokinetics, and safety indicators. Together, this combined experimental and computational approach aims to describe the anticancer potential of structurally distinct flavonoids and provide insights into their cell line–dependent activity in metastatic prostate cancer.

This study is the first to report that the flavonoid V3 can specifically give G2/M arrest of cell cycle in a p53-null prostate cancer cell line, exerting some selectivity for p53-null tumor cells. An ADMET analysis of flavonoids also confirmed the lead-like druglikeness of V3 and prioritizing it as the most suitable methoxylated flavonoid scaffold(s) for further validation. Moreover, this study goes beyond routine cytotoxicity and provides a competitive, mechanism-based comparison of structurally related flavonoids across metastatic prostate cancer cell models having genetically and metabolically different backgrounds.

2. Experimental

2.1. Chemicals and compounds used

The purified compounds from *Varthemia iphionoides* Boiss were kindly provided by the research group of Prof. Amal Al-Aboudi and Prof. Musa Abu Zarga at the University of Jordan, Jordan. These compounds were previously isolated and identified by Zerargui *et al.*[15] and the ethanolic extract was then partitioned between 10% aqueous methanol and hexane. The aqueous methanol layer was evaporated to dryness to obtain the crude extract, correspondingly. The purity of the compounds was confirmed based on HPLC analysis.[15] For all experiments, stock solutions were prepared in dimethyl sulfoxide (DMSO) and stored at −20 °C.

2.2. Cell culture

PC3 and DU145 human prostate cancer cell strains are sourced from American Type Culture Collection (ATCC, Manassas, Virginia, USA). The cells were cultivated in RPMI-1640 medium supplemented with 1% penicillin-streptomycin, 10% fetal bovine serum (FBS), and L-glutamine (all purchased from Sigma-Aldrich, St. Louis, MO, USA).The cells were maintained on T-75 culture flasks in a monolayer in an incubator (Sanyo, UK) at 37 °C, 5% CO_2, high humidity until they reaches 80–90% confluence. After that, the cells were detached by treating with 0.25% trypsin–EDTA solution and passaged again.

2.3. MTT assay

The anti-proliferative potential of the flavonoids was evaluated using the MTT (3-(4,5-dimethylthiazol-2-yl)-2,5-diphenyltetrazolium bromide; Sigma-Aldrich) colorimetric assay, as previously described,[16] to determine the half-maximal inhibitory concentration (IC_{50}) against prostate cancer cell lines. This method is based on the principle of viable cells reducing the yellowish tetrazolium salt to an insoluble dark purple formazan by the action of mitochondrial reductase enzymes. The released formazan represents a quick and reliable measure of the number of viable and dividing cells. Prostate cancer cells (20 000 cells per well) adhered in 96-well plates and were allowed to grow for 24 hours. Then cells were exposed to different concentrations of the test compounds in media containing DMSO at a final concentration of 0.1% in all conditions. After the treatment, the culture media was removed and 100 μL of a MTT solution was put into each well where phenol red-free media was used followed by 4 hours of incubation step. The resulting formazan crystals were dissolved in DMSO and

spectrophotometrically the absorbance was measured at 750 nm. The percentage cell viability was calculated using the following formula:-

$$\%\ \text{cell viability} = (\text{OD sample} - \text{OD blank}/\text{OD control} - \text{OD blank}) \times 100$$

Wherein, the blank corresponds to wells containing medium only (no cells), and the control represents untreated cells (considered 100% viable).

2.4. Mitochondrial membrane potential (MMP) assay

Mitochondrial membrane potential ($\Delta\Psi_m$) was determined using the Rhodamine 123 fluorescence (Sigma-Aldrich) assay, a well-established method for evaluating mitochondrial function.[17] PC3 and DU145 cells were cultured in 24-well plates at a quantity of 100 000 cells per well and allowed to stay on the cell culture for 24 hours. Following adherence, cells underwent serum starvation for an additional period of 24 hours in serum-free medium to synchronize cell cycles and minimize background signaling. To evaluate MMP, cells was then treated with two concentration of the compounds at 50 μM and 100 μM after which, the cells were treated at 37 °C with 10 μM Rhodamine 123 (Rh123) and 3 μM verapamil for 2 hours, the latter of which inhibits Rh123 efflux to facilitate dye retention. 3 μM Carbonyl cyanide *m*-chlorophenyl hydrazone (FCCP) (Sigma-Aldrich), a mitochondrial uncoupler, was employed as a positive control to disrupt $\Delta\Psi_m$. Following treatment, cells were rinsed with 1 mL of PBS per well to eliminate excess dye. To extract Rh123, 1 mL of destain solution (Roses destain: 50% water, 49% ethanol, and 1% acetic acid) was loaded to each well, and the plates were placed on a shaker for 10 minutes. The samples were then transferred to clear 96-well plates at a final volume of 200 μL per well in triplicates, and the fluorescence generated was measured using a spectrophotometric plate reader (Molecular Devices, CA). Rh123 accumulation was measured using a fluorescence plate reader, with excitation set at 485/20 nm and emission at 520/25 nm. The ratio was calculated between the fluorescence of treatments to that of control group and Rh123 uptake was indicated by the change in fluorescence whereby less intensity shows depolarized mitochondria.

2.5. Annexin V apoptosis assay

The cellular apoptosis rate was assessed using an eBioscience™ Annexin V-FITC Apoptosis Detection Kit, following the instructions provided by the manufacturer (Invitrogen™ BMS500FI-300). Briefly, cells were harvested after treatment, washed twice with cold phosphate-buffered saline (PBS, pH 7.4), and resuspended at 1 : 10 concentration in 1× binding solution relative to the volume of 10× supplied in the kit at a concentration of 1×10^6 cells per mL. A total of 1×10^5 cells were transferred to flow cytometry-compatible tubes and stained with 5 μL of Annexin V-FITC conjugate for 15 minutes at room temperature in the dark to detect phosphatidylserine (PS) externalization, an early marker of apoptosis. After Annexin V-FITC staining, PI staining solution was added to all the cooled tubes to a final concentration of 10 μL in each reaction mixture and the cells were left for an additional 5 minutes in the dark to demarcate late apoptotic and necrotic cells on the basis of membrane integrity. The cell suspensions were stained and then diluted with 400 μL of 1× binding buffer to optimize the flow cytometry measurement. Samples were analyzed immediately using Beckman Coulter's CytoFLEX S Flow Cytometer equipped with 488 nm excitation and appropriate filters for FITC (530/30 nm) and PI (585/42 nm) detection. Unstained cells, Annexin V-FITC-only, and PI-only controls were included to set up compensation and gating parameters. The percentage of viable cells (Annexin V-FITC-negative, PI-negative), early apoptotic cells (Annexin V-FITC-positive, PI-negative), late apoptotic cells (Annexin V-FITC-positive, PI-positive), and necrotic cells (Annexin V-FITC-negative, PI-positive) was quantified using Kaluza analysis software 2.3.

2.6. Cell cycle assay

Cell cycle distribution was analyzed by quantitating DNA content using propidium iodide (PI) staining, as previously described[18] with slight modifications. Briefly, approximately 1×10^6 cells were harvested, washed in cold phosphate-buffered saline (PBS), and resuspended in 0.5 mL of PBS. To obtain a mono-dispersed cell suspension and prevent aggregation, the sample was gently vortexed for 5 seconds or subjected to gentle pipetting with a Pasteur pipette. Cell fixation was performed by adding the cell suspension drop-wise to 4.5 mL of ice-cold 70% ethanol under gentle agitation. Fixed cells were stored at 4 °C for a minimum of 2 hours. Following fixation, cells were pelleted by centrifugation at 300*g* for 5 minutes and the ethanol supernatant was carefully decanted. The cell pellet was washed once with 5 mL PBS to remove residual ethanol, followed by another centrifugation step under identical conditions. For DNA staining, the cell pellet was resuspended in 0.5 mL of PI staining solution, containing 50 μg per mL propidium iodide and 100 μg per mL RNase A in PBS. Cells were incubated in the dark for 30 minutes at room temperature or for 10 minutes at 37 °C. Flow cytometric analysis was performed immediately using CytoFLEX S flow cytometer. PI fluorescence was excited using a 488 nm blue laser, and emission was collected using a 617 nm band-pass filter or a 610 nm long-pass filter, corresponding to its peak emission wavelength. Data analysis was performed *via* Kaluza analysis software 2.3.

2.7. Computational studies

Maestro v12.8.117 (Schrödinger Suite 2021–2) was used for computational prediction of physicochemical properties and ADMET profile (distribution, absorption, excretion, metabolism, and toxicity properties) of compounds V1–V7. The chemical structures were sketched in the maestro interface and prepared ligands using LigPrep tool[19] with defining the following parameters: Epik procedure was used to create ionization states at neutral pH (7.0 ± 0.4), and the chirality was determined from the 3D structure. After ligand preparation, Qik-prop tool[20] was used to compute the physicochemical properties and ADMET profiles, accordingly.

2.8. Data analysis

Data were analyzed using GraphPad Prism v10 Software (Inc., San Diego, CA, USA). All concentration response curves for the agonists were fitted using a four-parameter logistic nonlinear regression equation of the form:

$$E = E_{max}[A]^{nH}/EC_{50}{}^{nH} + [A]^{nH}$$

where [E] stands for the effect observed at the agonist concentration [A], [E_{max}] is the maximal response that can be produced by the drug, [nH] Hill slope, [EC_{50}] refers to the concentration of a ligand which induces a response halfway between the baseline and maximum response. pEC_{50} was defined as the negative logarithm of the EC_{50} value ($pEC_{50} = -\log EC_{50}$) in order to use the parametric tests for statistical comparisons. To account for variability from day to day and passage to passage, data were often normalized as a percentage of the positive control.

For the MTT assay, cell viability was calculated according to the formula:

$$\%\ \text{cell viability} = (\text{OD sample} - \text{OD blank}/\text{OD control} - \text{OD blank}) \times 100$$

where the blank is given by wells without cells (medium only), control is untreated cells (100% viable).

The normal distribution of data was assessed by D'Agostino-Pearson omnibus test and the data presented were reported as a mean ± standard error of the mean (SEM). At least 3 independent experiments performed in duplicate or triplicate as described. Statistical analysis between groups was performed using two-way ANOVA followed by Sidak multiple comparisons or one-way ANOVA followed by Dunnett multiple comparisons. To measure the difference between two samples, paired or unpaired two-tailed Student's t-test was used where applicable. The level of uncertainty in rejecting the null hypothesis was indicated by significance values; P values ≤ 0.05 were determined to be significant where $^{*}p < 0.05$, $^{**}p < 0.01$, $^{***}p < 0.001$, and $^{****}p < 0.0001$, respectively.

3. Results and discussion

3.1. Cytotoxic activity of flavonoids on PC3 and DU145 cell lines

The flavonoids isolated from Varthemia iphionoides were tested for their cytotoxic activity against two human prostate cancer cell lines, PC3 and DU145. The assessment of the potency and efficacy of each compound was based on the determination of their IC_{50} (half-maximal inhibitory concentration) and E_{max} (maximum effect) values, respectively (Table 1). In PC3 cells, santin (V4) exhibited the highest potency with an IC_{50} of 2.08 ± 0.09 μM, followed by jaceidin (V1) (2.91 ± 0.10 μM) and quercetin-3,3′-dimethyl ether (V5) (5.16 ± 0.13 μM). Kumatakenin (V2) has showed the lowest potency (IC_{50} = 13.81 ± 0.22 μM). In terms of efficacy, santin (V4) had the highest Emax value (79.56 ± 3.84%) whereas jaceidin (V1) and viscosine (V6) gave quite similar Emax values 78.00 ± 4.44% and 74.33 ± 2.72%, respectively. In DU145 cells, kumatakenin (V2) demonstrated the highest potency (IC_{50} = 0.23 ± 0.12 μM), followed by 4′-hydroxy-3,5,6,7-tetramethoxyflavone (V3) (1.30 ± 0.69 μM) and quercetin-3,3′-dimethyl ether (V5) (4.27 ± 1.27 μM). Santin (V4), which was the strongest in PC3 cells, surprisingly showed less potency in DU145 cells (IC_{50} = 13.54 ± 3.55 μM). However, it should be mentioned that the activity of santin (V4) on PC3 cells was very low and yet it was able to nearly totally inhibit viability of cells in DU145 cells (96.29 ± 6.82%). Quercetin-3,3′-dimethyl ether (V5) and jaceidin (V1) also demonstrated high efficacy (E_{max} = 85.39 ± 5.68% and 80.09 ± 5.35%, respectively), while kumatakenin (V2), despite its high potency, showed the lowest efficacy (E_{max} = 43.53 ± 6.76%). The diverse anticancer effects of these flavonoids, which are chemically related, highlight their selective mechanisms of action that can be highly influenced by the particular cellular environment of different prostate cancer subtypes. These values are in the same range of those reported for other methoxylated flavonoids in prostate cancer models[21] and are in the medium potency range that is characteristic of natural products but which may be compensated by their safety profile. Normal-cell cytotoxicity testing was previously performed in a normal fibroblast cell line and showed no significant toxicity.[22] Concentration–response curves for all compounds are shown in Fig. 2.

The observed differential treatment efficacy between the two cell lines emphasizes tumor heterogeneity and corresponds well with the biological differences observed between prostate cancer metastases.[23,24] MTT cytotoxicity determined structure–activity relationships (SAR) and cell line-dependent potency, a recurring trend observed in testing natural products against heterogeneous cancer cell models.[25] For example, Jaceidin (V1) is reported to induce apoptotic cell death in human ovary cancer cells by mitochondrial potential collapse.[26] Although

Table 1 Comparative IC_{50} (half-maximal inhibitory concentration) and E_{max} (maximal effect) values of flavonoids (V1–V6) on PC3 and DU145 prostate cancer cells

Compound	PC3 $IC_{50}{}^{a}$ (μM)	PC3 $E_{max}{}^{a}$ (%)	DU145 $IC_{50}{}^{a}$(μM)	DU145 $E_{max}{}^{a}$(%)
V1	2.91 ± 0.10	78.00 ± 4.44	7.23 ± 1.79	80.09 ± 5.35
V2	13.81 ± 0.22	54.42 ± 7.55	0.23 ± 0.12	43.53 ± 6.76
V3	7.22 ± 0.21	69.89 ± 8.00	1.30 ± 0.69	66.50 ± 7.79
V4	2.08 ± 0.09	79.56 ± 3.84	13.54 ± 3.55	96.29 ± 6.82
V5	5.16 ± 0.13	69.70 ± 4.77	4.27 ± 1.27	85.39 ± 5.68
V6	7.43 ± 0.07	74.33 ± 2.72	6.13 ± 3.58	79.52 ± 10.83

[a] Data are presented as mean ± SEM of $N = 3$ independent biological replicates, each is the average of three technical replicates.

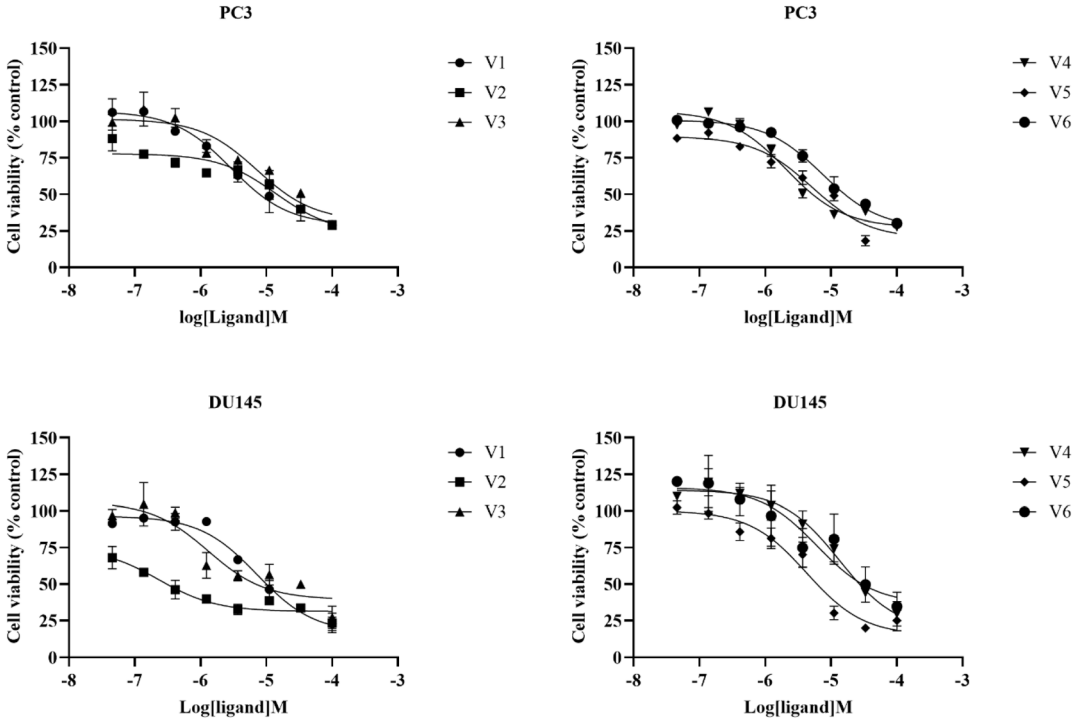

Fig. 2 Concentration-response curves of compounds V1–V6 on prostate cancer cell lines (PC3 and DU145). Cells were treated with increasing concentrations of each compound for 48 h. Data are expressed as mean ± SEM of $N = 3$ independent biological replicates, each is the average of three technical replicates.

kumatakenin (V2) has no reports against cancer, it exhibits anti-inflammatory and antioxidant properties that can indirectly contribute to its anticancer efficacy. Santin (V4) is documented as a caspase-dependent apoptotic mitochondrial dysfunction inducer.[27] Similarly, V5, a methylated quercetin analog, has been reported to exhibit higher metabolic stability and anti-proliferative potentials against cancer cells.[28] These reports point towards the fact that minor variations cause cell line-specific sensitivities.

3.2. Flavonoids affect mitochondrial membrane potential (MMP)

The effects of the flavonoids on MMP were evaluated in DU145 and PC3 prostate cancer cell lines using the rhodamine 123 assay (Table 2). FCCP (3 μM), a known mitochondrial uncoupler, was served as a positive control and induced a significant reduction in MMP in both PC3 (18.5 ± 0.99) and DU145 (32.75 ± 0.24) cells, respectively. In PC3 cells, at 50 μM, V1 (68.6 ± 1.36) and V4 (66.52 ± 2.70) exhibited the highest fluorescence intensities, indicating relatively preserved MMP, whereas V3 (41.81 ± 0.68) and V6 (25.14 ± 0.32) caused substantial reductions, indicating a pronounced mitochondrial depolarization. At an elevated concentration of 100 μM, all flavonoids elicited further declines in MMP, with V3 (23.28 ± 0.62) and V6 (27.31 ± 0.52) demonstrating the potential anticancer effects. The compounds V1 and V4 demonstrated concentration-dependent reductions (40.72 ± 5.29 and 53.25 ± 0.83, respectively), while V2, V5, and V7 provoked significant decrease in the potency (38.10 ± 0.07, 34.90 ± 0.86, and 31.63 ± 0.72, respectively). In DU145 cells, a similar trend of potency was observed. At 50 μM, V1 (62.79 ± 0.55) and V6 (63.84 ± 0.64) maintained the highest MMP

Table 2 The effect of flavonoids and reference compound (FCCP) on MMP in DU145 cells

Compound	PC3 [a](50 μM)	PC3 [a](100 μM)	DU145 [a](50 μM)	DU145 [a](100 μM)
FCCP (3 μM)	18.5 ± 0.99	—	32.75 ± 0.24	—
V1	68.6 ± 1.36	40.72 ± 5.29	62.79 ± 0.55	39.76 ± 0.97
V2	54.42 ± 1.69	38.10 ± 0.07	36.33 ± 0.87	31.56 ± 0.31
V3	41.81 ± 0.68	23.28 ± 0.62	40.37 ± 10.16	25.08 ± 0.23
V4	66.52 ± 2.70	53.25 ± 0.83	53.33 ± 0.47	43.93 ± 0.55
V5	52.94 ± 1.23	34.90 ± 0.86	43.94 ± 0.46	41.26 ± 0.62
V6	25.14 ± 0.32	27.31 ± 0.52	63.84 ± 0.64	51.47 ± 0.83

[a] Data are presented as mean ± SEM of $N = 3$ independent biological replicates, each is the average of three technical replicates.

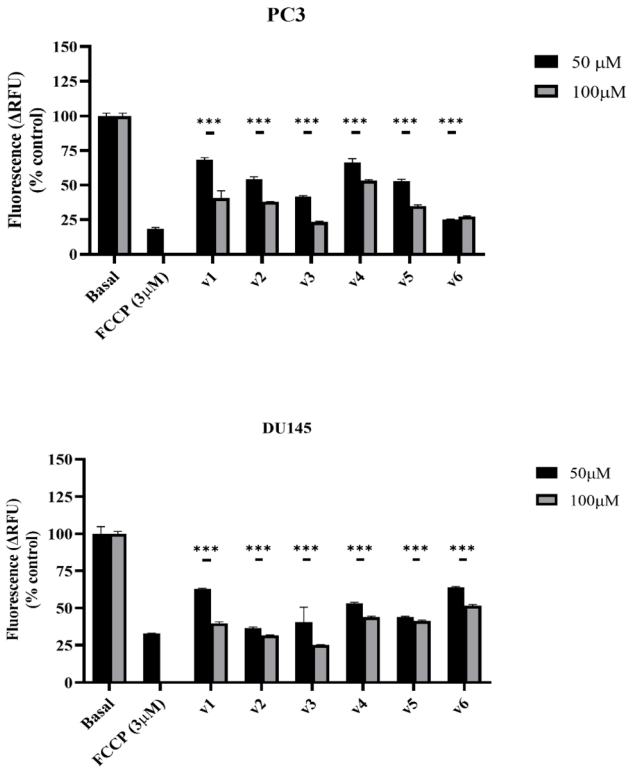

Fig. 3 Effects of flavonoids on mitochondrial membrane potential (MMP) in PC3 and DU145 prostate cancer cell lines. MMP was assessed using rhodamine 123 fluorescence intensity, expressed as relative fluorescence units (RFU), and normalized to the untreated control group (100%). Lower percentages indicate greater MMP depolarization. Cells were treated with two concentrations (50 μM and 100 μM) of each compound. Data are presented as mean ± SEM of $N = 3$ independent biological replicates, each is the average of three technical replicates. Statistical significance ($p < 0.05$) of treatment effect compared to control (untreated cells) was determined using two-way ANOVA with Sidak's multiple comparisons test. ***$p < 0.001$.

levels, whereas V2 (36.33 ± 0.87) and V3 (40.37 ± 10.16) induced more significant reductions. At 100 μM, V3 (25.08 ± 0.23) and V2 (31.56 ± 0.31) continued to exhibit the strongest MMP disruption. Other compounds like V1, V4, V5, V6, and V7, also significantly reduced MMP (39.76 ± 0.97, 43.93 ± 0.55, 41.26 ± 0.62, 51.47 ± 0.83, and 47.85 ± 0.19, respectively). These findings demonstrated that the tested flavonoids exert concentration-dependent effects on mitochondrial function, with V3 and V6 consistently manifesting the most potent mitochondrial depolarizing effects across the two prostate cancer cell lines (Fig. 3).

3.3. Flavonoid induces apoptosis in PC3 and DU145 prostate cancer cells

To evaluate the pro-apoptotic potential of the flavonoid compounds, PC3 and DU145 prostate cancer cell lines were treated and evaluated *via* flow cytometry employing Annexin V-FITC and propidium iodide (PI) staining, quantitatively. The results showed a unique apoptosis response (Fig. 4) depending on the cell line for the compounds V3, V5, and V6 (Table 3). In PC3 cells, compounds V3 and V6 induced early apoptosis effectively, with rates of 11.20 ± 1.20% and 9.95 ± 0.95%, respectively, representing a substantial increase over the vehicle control (0.40 ± 0.12%). These compounds also significantly elevated late apoptotic populations (V3: 4.55 ± 0.55%; V6: 4.25 ± 0.25%), culminating in total apoptosis rates of 15.75 ± 1.75% for V3 and 14.20 ± 1.20% for V6 compared to control (0.65 ± 0.25%). The mitochondrial membrane potential (MMP) results are in line with these findings and emphasizing that V3 and V6 provoke apoptosis through mitochondrial destruction. In particular, the compound V5 showed a unique apoptotic profile in PC3 cells. Late apoptosis (8.95 ± 0.95%) was significantly increased when compared with early apoptosis (1.40 ± 0.20%). The compound V5 also accounted for the total apoptotic effect of 10.35 ± 1.15% indicating its strong anticancer activity. On the contrary, the DU145 cells had a dramatically reduced response to all the three compounds. The V3 and V6 treatments caused a significant rise in total apoptosis (5.50 ± 0.20% and 5.97 ± 0.64%, respectively) when compared to the control group (1.90 ± 0.10%), However, the degree of these effects was almost 3 times lesser than that observed in PC3 cells. Compound V5 initiated a small but steady apoptotic reaction in DU145 cells (5.00 ± 0.10%), which was in contrast with its stronger effect in PC3 cells.

The PC3 and DU145 cell lines' exhibited different sensitivity pointing the importance of cellular context in apoptosis due to flavonoids, possibly indicating different genetic backgrounds that distinguish these prostate cancer models. Hence, based on the obtained results, it can be concluded that compounds V3 and V6 are selective to inducing apoptosis in PC3 cells, suggesting the heterogeneity of these two cell lines in terms of mitochondrial integrity, oxidative stress and apoptotic signaling pathways, which are the main reasons for the differences in treatment performance. The different reactions reveal how much tumor diversity affects the effectiveness of the compound. Moreover, these results imply that V3 and V6 more likely trigger early apoptosis, while V5 leads to the late apoptotic phenotype, thus showing possible mechanistic diversity (Fig. 5). The great sensitivity of PC3 cells designates that the tested compounds might be especially effective against aggressive prostate cancer phenotypes with dysfunctional p53 pathways.

Mitochondria were chosen as a primary intracellular target for these drug discovery leads. Compounds V3, V5, and V6 significantly depolarized MMP, which is corroborated well with the finding that methoxylated flavones could directly impair mitochondrial function.[10] Consequently, the decline of MMP was correlated with the increased Annexin V/PI staining of cells, indicating programmed cell death *via* intrinsic pathway.[29] Previous reports have indicated multiple flavonoids in arresting variably the Bcl-2 family proteins and cytochrome C release in mitochondria.[30] Moreover, it was determined that PC3 cells were more prone to apoptosis mediated by the mitochondria than DU145 cells, This correlate with the fact that PC3 cells have a higher basal ROS level and are more reliant on oxidative metabolism.[22]

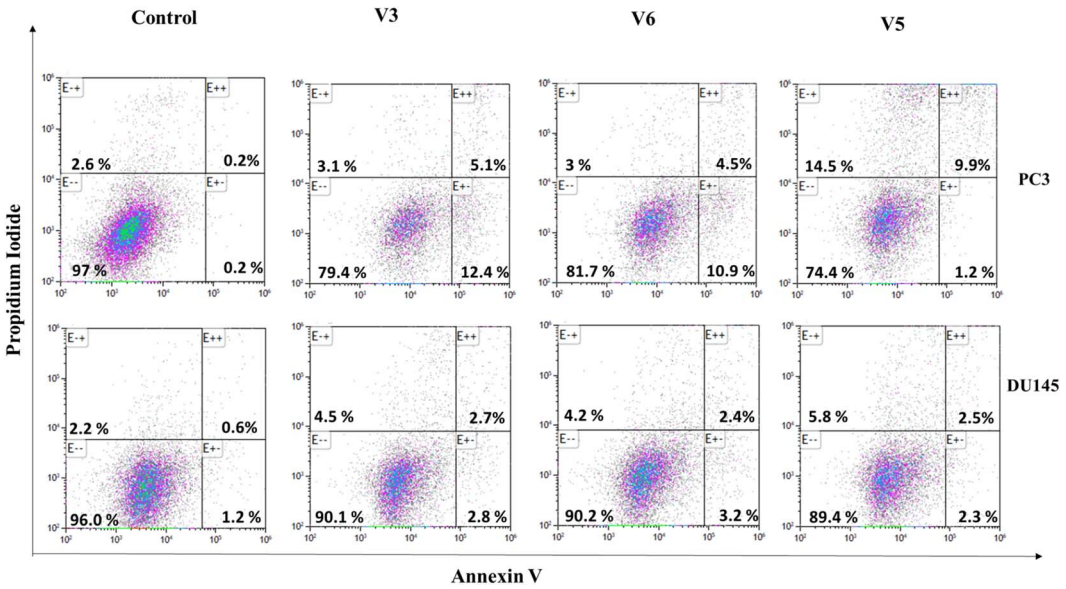

Fig. 4 The representative dot plots display how the viable cells (Annexin V^-/PI^-), early apoptotic cells (Annexin V^+/PI^-), late apoptotic cells (Annexin V^+/PI^+), and necrotic cells (Annexin V^-/PI^+) were distributed after the 24-hours treatment. The control group was treated with the vehicle only. Effect of selected compounds (V3, V5, and V6) on apoptosis induction in PC3 and DU145 prostate cancer cells as assessed by Annexin V/Propidium Iodide.

3.4. Flavonoids induce cell cycle arrest in PC3 and DU145 cells

Propidium iodide-based flow cytometry was used to quantify the impact of the flavonoid derivative V3 on cell cycle progression in the prostate cancer cell lines PC3 and DU145. A 10 μM V3 treatment caused the cell lines to undergo different arrest patterns that were highly specific, thus implying different mechanisms of action in each model (Fig. 6). In PC3 cells, the treatment with V3 for 24 hours almost doubled the percentage of cells in the G2/M phase, up from the baseline of 16.4 ± 1.2% to 38.7 ± 1.8%. This was followed by proportional reductions in G0/G1 (55.2 ± 2.1% to 42.1 ± 1.6%) and S phase populations (28.4 ± 1.5% to 19.2 ± 1.3%). On the other hand, the DU145 responded to V3 with the gradual arrest of cells in S phase. Following 24-hours treatment, the S phase population increased from 23.7 ± 1.4% to 35.6 ± 1.7%, with reductions in both G0/G1 (58.6 ± 2.3% to 44.2 ± 1.8%) and G2/M populations (17.7 ± 1.1% to 20.2 ± 1.0%). These data suggest that V3 causes severe disruption of cell cycle progression in both cell lines through different pathways: G2/M phase arrest for PC3 and S phase arrest for DU145 (Fig. 6 and Table 4). The presence of sub-G1 populations in both models suggested that cell cycle arrest ultimately leads to apoptotic cell death. The different responses highlighted the cell line-specific activity of V3, most probably due to the distinct molecular profiles of the different prostate cancer models.

A remarkable observation was made that V3 could still cause cell cycle arrest, albeit in a cell line-dependent way. Strong G2/M arrest was seen in the p53-null PC3 cells that were treated with V3, indicating either the disruption of mitotic spindle assembly

Table 3 Effects of V3, V6, and V5 on early, late, and total apoptosis in PC3 and DU145 prostate cancer cells[a]

Condition	Early apoptosis (%, mean ± SEM)	Late apoptosis (%, mean ± SEM)	Total apoptosis (%, mean ± SEM)
PC3			
Control	0.4 ± 0.12	0.25 ± 0.05	0.65 ± 0.25
V3	11.20 ± 1.2	4.55 ± 0.55	15.75 ± 1.75
V6	9.95 ± 0.95	4.25 ± 0.25	14.20 ± 1.20
V5	1.40 ± 0.20	8.95 ± 0.95	10.35 ± 1.15
DU145			
Control	1.25 ± 0.05	0.65 ± 0.05	1.90 ± 0.10
V3	2.90 ± 0.10	2.60 ± 0.10	5.50 ± 0.20
V6	3.70 ± 0.50	2.27 ± 0.14	5.97 ± 0.64
V5	1.25 ± 0.05	0.65 ± 0.05	1.90 ± 0.10

[a] Cells were stained with Annexin V-FITC and propidium iodide and analyzed by flow cytometry. Data represent the mean ± SEM of 3 independent experiments, each performed in duplicates.

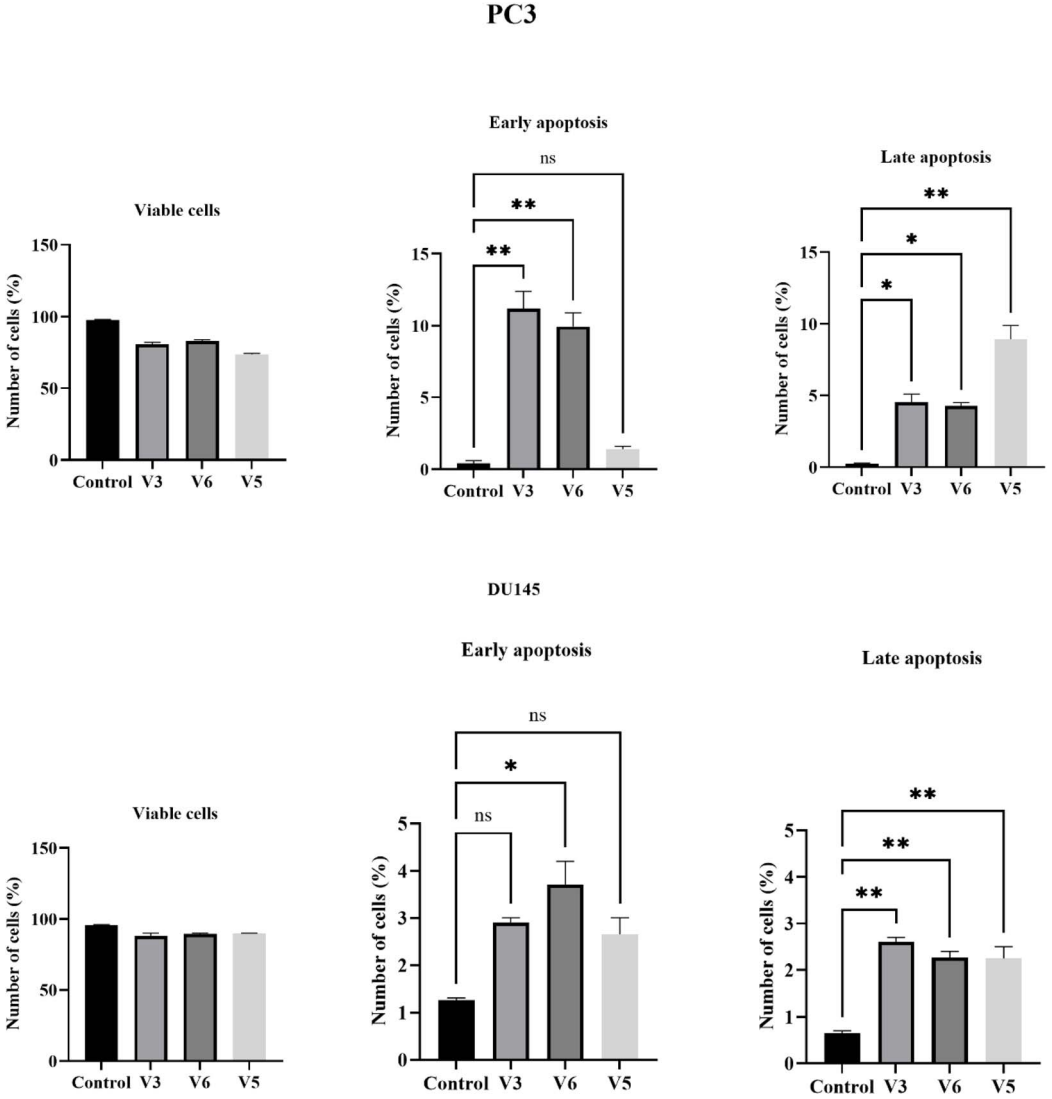

Fig. 5 Annexin V/PI analysis of apoptosis in PC3 and DU145 prostate cancer cells treated with flavone derivatives. DU145 cells were treated with 10 μM V3 (4′-hydroxy-3,5,6,7-tetramethoxyflavone), V5, or V6 for 24 h and stained with Annexin V-FITC/propidium iodide. Flow cytometric analysis quantified the percentage of viable, early apoptotic, and late apoptotic cells. Data were analyzed by two-way ANOVA with Sidak multiple comparisons test. Data are expressed as mean ± SEM of three independent experiments performed in triplicate. *$p < 0.05$, **$p < 0.01$; ns, not significant.

or activation of DNA damage checkpoints.[31] In contrast, DU145 cells (with wild-type p53) demonstrated an S-phase perturbation, thereby pointing out the influence of p53 status on determining if checkpoint fidelity is maintained.[32] The increase in the number of cells in the sub-G1 fraction suggests that cell cycle arrest likely precedes apoptotic death. Methoxylated flavones including tetramethoxyflavones have reported to exhibit similar arrest phenotypes in colon and breast tumor models. Therefore, our results are in good alignment with the already established flavonoid-induced cyclin responsive arrest of cell line models.[21] The differential G2/M and S phase arrest described here in the p53 null PC3 and wild-type p53 DU145 cells have demonstrated the dependence of cell cycle arrest on p53 status and methoxylation in flavonoids.

The study revealed that in response to V3, a different checkpoint response is induced depending on the cell type. Moreover, the increase of cells in the sub-G1 fraction also indicates that after cell cycle arrest apoptotic death occurs. Methoxylated flavonoids target mitochondria, and in the case of tetramethoxyflavones, apoptosis is induced.[10] Therefore, this finding has important clinical implications and would require the development of patient-specific approaches in flavonoid-containing cancer treatment regimens. Remarkably, the ability to target both mitochondria and the cell cycle could be a valuable strategy to avoid resistance mechanisms, which are commonly seen in metastatic prostate cancer cells.[24]

3.5. Computational studies

3.5.1. Evaluation of drug-likeness and physicochemical properties. A thorough *in silico* investigation of the physicochemical and drug-like properties of the flavonoids (V1–V6) was

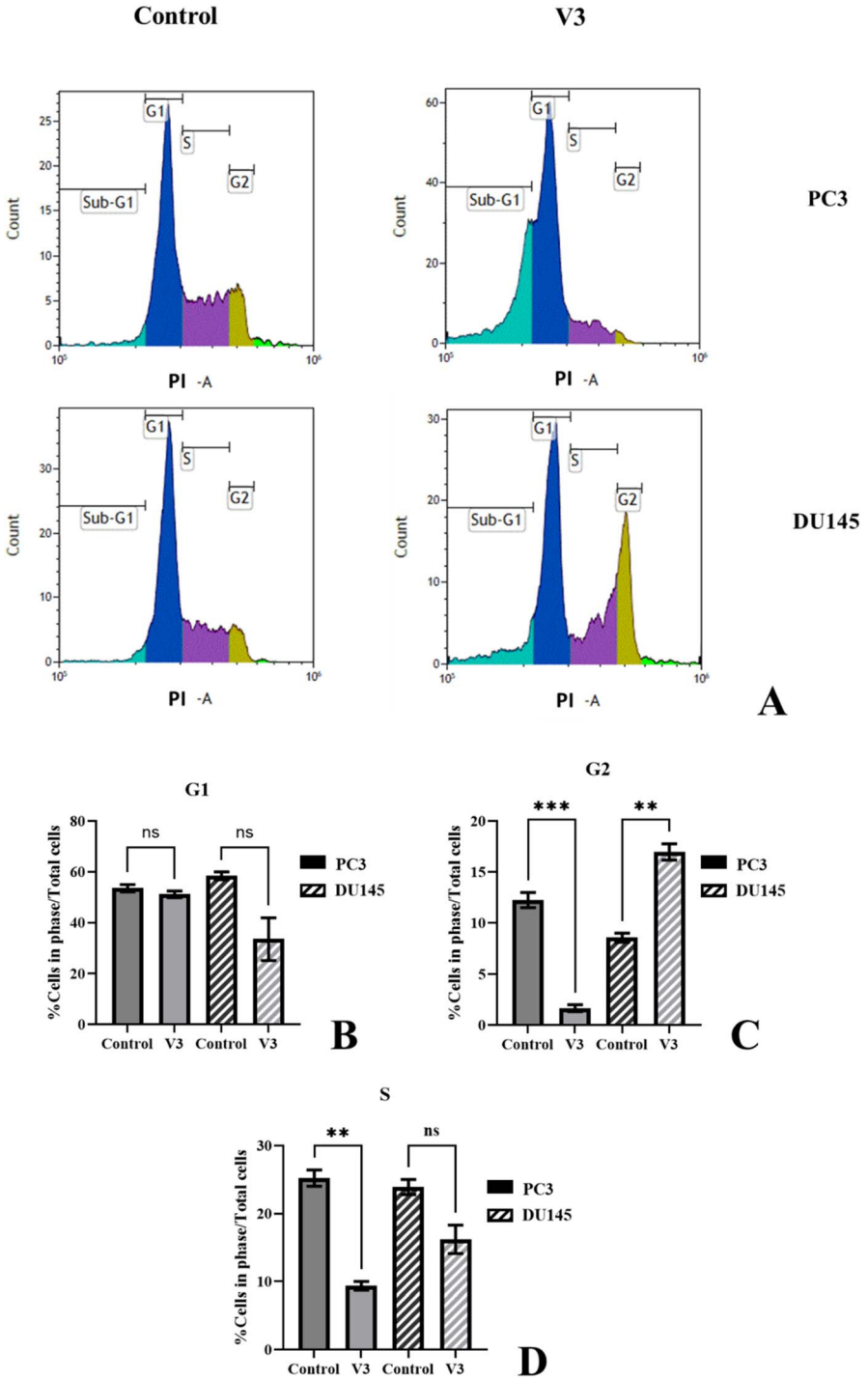

Fig. 6 Cell cycle profile following treatment with flavonoids V3. (A) A representative Kaluza cell cycle histogram of PI-stained PC3 and DU145 cells following 24 h-treatment of flavonoid V3 (10 μM) compared to untreated controls. (B–D) Progression of cell cycle phases assessed using ordinary one-way ANOVA with Dunnett's multiple comparisons test. Bars represent mean ± SEM of 2 independent biological replicates.

performed and collected the results in Table 5. All compounds revealed good agreement of drug-likeness criteria of Lipinski's Rule of Five and Jorgensen's Rule of Three, with the number of property outliers to be within the acceptable range (0–5). Each compound exhibited optimal molecular characteristics of molecular weight, number of rotatable bonds, hydrogen bond donors/acceptors, and globularity favorable to oral bioavailability. Particularly, the most potent compounds identified in the biological assays—V3, V5, and V6—owned additional advantages. The dipole moments and solvent-accessible surface areas calculated for V3, V5, and V6 were highly favorable to the effective membrane interaction and target engagement, thus,

Table 4 Effect of V3 on cell cycle distribution in PC3 and DU145 prostate cancer cells[a]

Cell line	Phase	Control (mean ± SEM)	V3 (mean ± SEM)
PC3	Sub-G1	3.28 ± 0.28	23.61 ± 0.49
	G1	53.55 ± 1.46	51.14 ± 1.32
	S	25.21 ± 1.21	9.37 ± 0.63
	G2/M	12.26 ± 0.75	1.66 ± 0.34
DU145	Sub-G1	3.85 ± 0.15	19.45 ± 1.31
	G1	58.46 ± 1.55	33.55 ± 8.37
	S	23.89 ± 1.11	16.22 ± 2.10
	G2/M	8.56 ± 0.45	16.98 ± 0.81

[a] Data are presented as mean ± SEM from replicate experiments. Sub-G1 indicates apoptotic population, while G1, S, and G2/M represent distinct phases of the cell cycle.

a structural rationale for their strong potency in causing mitochondrial membrane depolarization, apoptosis, and cytotoxicity in PC3 and DU145 prostate cancer cell lines was given, effectively.

3.5.2. *In silico* ADMET profiling. To assess the suitability of using as orally bioavailable drugs, the ADMET profiles of V1 to V6 were computed and presented in Table 6. The lead compound V3, displayed significant permeability, with Caco-2 and MDCK with values of 1526.37 and 781.39 nm s^{-1}, respectively, suggesting of conferring to high intestinal absorption and blood–brain barrier permeation. Its pharmacokinetic profile had an optimal balance of properties: a moderate logP value (3.12), high predicted human oral absorption (100%), and acceptable aqueous solubility ($\log S = -4.33$). Most notably, V3 was predicted to have a high safety margin with no HERG channel inhibition liability ($pIC_{50} = -5.10$). The computed CNS activity score of 0 specifies that there will be no central nervous system exposure which is a beneficial factor for its expectant peripheral mechanism of action, devoid of CNS toxicity. Compounds V5 and V6 exhibited good ADMET properties with reasonable oral absorption (>75%) and fair permeability, although they displayed lower solubility. The optimal pharmacokinetic and safety data unequivocally favors to further studies on potential compounds V3, V5, and V6.

Experimental and computational techniques were integrated to identify a series of flavonoid-based compounds (VA3, VA5, and VA6) as promising lead structures with significant anti-tumor therapeutic potential. These compounds markedly induced mitochondrial dysfunction and apoptosis in highly aggressive prostate cancer cells and possessed favorable drug-like and ADMET properties. Among them, V3 showed the most promising profile since, V3 was able to better predict oral bioavailability, minimal toxicity, and peripherally selective distribution, crucial for translation into preclinical and clinical development stages.

The adherence of these compounds to essential drug-likeness principles significantly reduces development risks. VA3 has the best pharmacokinetic profile with a high predicted permeability (Caco-2: 1526.37 nm s^{-1}), complete human oral absorption (100%), a balanced log *P* value (3.12), and adequate solubility ($\log S$ −4.33). All of these factors suggest that it has a strong potential for effective oral bioavailability. These parameters are in line with recent literature for antioxidant flavonoids evaluated for drug-likeness and pharmacokinetics by using SwissADME and DFT analysis.[33] The limited CNS activity is advantageous as it diminish the neurological adverse effects, while preserving efficacy against peripheral malignancies. From the *in silico* profile, one would then predict V3 to be the best mitochondrial targeting drug with the least toxicity and greatest selectivity against cancer cells, while V5 and V6 would have utility as chemoprotective agents. However, further biophysical verification would be required before translation to the clinic.

Together, this study identifies V3 as a promising mitochondria-targeting flavonoid with selective anticancer activity against aggressive prostate cancer models. By integrating functional assays with predictive ADMET modelling, this work establishes a translational framework for advancing flavonoid-based therapeutics tailored to tumour-specific vulnerabilities. These findings support further preclinical evaluation of V3 and highlight the importance of incorporating

Table 5 Prediction of drug-likeness, physicochemical, and molecular properties for all compounds (V1–V6)

Property	Recommended range	V1	V2	V3	V4	V5	V6
No. of properties outside the 95% range for known drugs	0–5	**0**	**0**	**0**	**0**	**0**	**0**
Rotatable bonds	0–15	6	4	5	5	5	4
Molecular weight (g mol^{-1})	130–725	360.32	314.294	358.347	344.32	330.293	300.267
Dipole moment (Debye)	1.0–12.5	6.042	3.48	4.744	5.519	5.227	2.941
Solvent accessible surface area ($Å^2$) (SASA)	300–1000	570.606	546.858	610.774	575.551	584.445	523.326
Hydrophobic component of SASA (FOSA)	0–750	229.278	173.217	332.593	257.909	160.179	80.606
Hydrophilic component of SASA (FISA)	7.0–330.0	169.395	135.68	85.652	116.027	190.922	190.45
π-Component of SASA (PISA)	0–450	171.933	237.961	192.529	201.615	233.344	252.271
Weakly polar surface area (WPSA)	0–175.0	0	0	0	0	0	0
Molecular volume ($Å^3$)	500–2000	1020.377	945.23	1085.421	1014.787	998.203	893.836
H-bond donors	0–6	2	1	1	1	2	2
H-bond acceptors	2 – 20	6	4.5	6.25	5.25	5.25	4.5
Globularity (spherical = 1.0)	0.75–0.95	0.859019	0.851757	0.836276	0.848525	0.826484	0.857494
Lipinski rule violations (rule of five)	Max 4	**0**	**0**	**0**	**0**	**0**	**0**
Jorgensen's rule violations (rule of three)	Max 3	**0**	**0**	**0**	**0**	**0**	**0**

Table 6 Prediction of ADMET (absorption, bistribution, metabolism, excretion, toxicity) Properties for all compounds (V1–V6)

Description	Recommended range	V1	V2	V3	V4	V5	V6
Octanol/water partition (log P_o/w)	−2.0–6.5	2.119	2.68	3.119	2.882	2.166	1.852
Aqueous solubility (log S)	−6.5–0.5	−3.595	−3.968	−4.326	−4.067	−4.196	−3.539
Conformation-independent solubility (CIlog S)	−6.5–0.5	−5.067	−4.765	−4.965	−5.077	−4.751	−4.429
HERG K^+ channel blockage log(IC50)	Concern below −5	−4.633	−5.066	−5.099	−4.945	**−5.452**	**−5.041**
Brain/blood partition (logBB)	−3.0–1.2	−1.329	−0.924	−0.554	−0.812	−1.601	−1.404
Caco-2 permeability (nm s^{-1})	<25 poor; >500 great	245.205	511.973	1526.372	**786.351**	153.247	154.833
MDCK permeability (nm s^{-1})	<25 poor; >500 great	108.269	239.928	**781.385**	381.526	65.141	65.87
Skin permeability (log K_p)	−8.0 to −1.0	−3.46	−2.798	−1.94	−2.468	−3.736	−3.757
Binding to human serum albumin (log K_{hsa})	−1.5–1.5	−0.004	0.161	0.144	0.158	0.081	−0.003
Human oral absorption	1 (low), 2 (medium)	**3**	**3**	**3**	**3**	**3**	**3**
Human oral absorption percentage (%)	>80% high	82.12	91.127	100	95.645	78.744	76.983
Predicted metabolic reactions	1–8	6	4	5	5	5	4
Max. Transdermal transport rate	—	0.032	0.051	0.194	0.1	0.004	0.015
Predicted CNS activity (scale)	−2 (inactive) to +2 (active)	−2	−1	0	−1	−2	−2
Reactive functional groups	0–2	**0**	**0**	**0**	**0**	**0**	**0**

tumour heterogeneity into natural product–based drug discovery strategies.

While flavonoids and several methoxylated analogues have been previously reported to exhibit anticancer activities, the novelty of the present work lies in its comparative, mechanism-resolved, and heterogeneity-aware evaluation of six structurally diverse flavonoids isolated from Varthemia iphionoides specifically in metastatic prostate cancer models. Rather than reiterating descriptive cytotoxic screening, this study integrates mitochondrial functional readouts ($\Delta\Psi_m$ depolarization), apoptosis quantification, and cell-cycle profiling across two biologically distinct metastatic cell lines (PC3 and DU145) to delineate context-dependent vulnerabilities and establish structure–mechanism relationships. Importantly, our data provide evidence that a tetramethoxyflavone (V3) induces divergent checkpoint responses linked to p53 background, alongside consistent mitochondrial dysfunction and apoptosis, thereby offering mechanistic insight into how genetically distinct metastatic tumors may respond differently to mitochondria-targeting natural products. In addition, coupling these functional findings with *in silico* pharmacokinetic/ADMET profiling advances the work from "activity reporting" toward a translational prioritization framework, identifying V3 (and to a lesser extent V5 and V6) as lead candidates with drug-like properties suitable for downstream preclinical development. Collectively, the study's contribution is not the first mention of flavonoids as anticancer agents, but the first integrated demonstration—within this compound set and disease context—of mechanistic stratification across metastatic models, which is essential for rational advancement of natural-product scaffolds in precision-oriented prostate cancer therapeutics.

4. Conclusion

This study provides a comprehensive mechanistic evaluation of the anticancer efficacy of six structurally distinct flavonoids isolated from *Varthemia iphionoides* toward metastatic prostate cancer cell lines, PC3 and DU145. Findings revealed that these compounds exert their effects by causing mitochondrial dysfunction, cell cycle arrest, and subsequent apoptotic cell death in metastatic cells. Among all the compounds tested, 4′-hydroxy-3,5,6,7-tetramethoxyflavone (V3), quercetin-3,3′-dimethyl ether (V5), and viscosine (V6) emerged as potential anticancer leads. Moreover, This is the first report to show a p53 dependent divergence in cell cycle regulation exerted by tetramethoxyflavone (V3) with mitochondrial dysfunction and further support from superior *in silico* pharmacokinetic profiles. This study goes beyond routine cytotoxicity and provides a competitive, mechanism-based comparison of structurally related flavonoids across metastatic prostate cancer cell models having genetically and metabolically different backgrounds.

Author contributions

Conceptualization: W.·H.; conducted all experiments: W.·H.; investigation: W.·H.; formal analysis: W.·H.; data curation: W.·H.; writing—original draft, and writing—review & editing: W.·H.; visualization and project administration: W·.H.

Conflicts of interest

The author declares no competing interests.

Data availability

The data supporting the findings of this study are available within the article. Additional raw data can be provided by the corresponding author upon reasonable request.

Acknowledgements

The author thank the Deanship of Scientific Research and Graduate Studies, Philadelphia University, for providing the

fund (Grant Number 100/34/541/2022). The flavonoid compounds used in this study were kindly provided by Professors Amal Al-Aboudi and Musa Abu Zarga of the University of Jordan's Department of Chemistry. Additionally, I would like to thank the University of Nottingham Medical School (United Kingdom) for providing the necessary facilities, equipment, and analysis software to perform this study.

References

1 R. Raychaudhuri, D. W. Lin and R. B. Montgomery, *JAMA*, 2025, **333**, 1433–1446.
2 B. Liu, H. Zhou, L. Tan, K. T. H. Siu and X. Y. Guan, *Signal Transduction Targeted Ther.*, 2024, **9**, 175.
3 H. Hasnat, S. A. Shompa, M. M. Islam, S. Alam, F. T. Richi, N. U. Emon, S. Ashrafi, N. U. Ahmed, M. N. R. Chowdhury, N. Fatema, M. S. Hossain, A. Ghosh and F. Ahmed, *Heliyon*, 2024, **10**, e27533.
4 S. A. Mir, A. Dar, L. Hamid, N. Nisar, J. A. Malik, T. Ali and G. N. Bader, *Curr. Res. Pharmacol. Drug Discovery*, 2024, **6**, 100167.
5 A. Hosseinzadeh, F. Poursoleiman, A. N. Biregani and A. Esmailzadeh, *Cancer Cell Int.*, 2023, **23**, 114.
6 P. A. Silva-Pinto, J. T. C. de Pontes, B. Aguilar-Morón, C. S. C. Canales, F. R. Pavan and C. A. Roque-Borda, *Heliyon*, 2025, **11**, e42682.
7 Q. Wang, Y. Yuan, J. Liu, C. Li and X. Jiang, *Front. Immunol.*, 2024, **15**, 1520072.
8 J. D. Ly, D. R. Grubb and A. Lawen, *Apoptosis*, 2003, **8**, 115–128.
9 A. Liskova, M. Samec, L. Koklesova, A. Brockmueller, K. Zhai, B. Abdellatif, M. Siddiqui, K. Biringer, E. Kudela, M. Pec, L. K. Gadanec, M. Šudomová, S. T. S. Hassan, A. Zulli, M. Shakibaei, F. A. Giordano, D. Büsselberg, O. Golubnitschaja and P. Kubatka, *EPMA J.*, 2021, **12**, 155–176.
10 H. Slika, H. Mansour, N. Wehbe, S. A. Nasser, R. Iratni, G. Nasrallah, A. Shaito, T. Ghaddar, F. Kobeissy and A. H. Eid, *Biomed. Pharmacother.*, 2022, **146**, 112442.
11 N. Lotfi, Z. Yousefi, M. Golabi, P. Khalilian, B. Ghezelbash, M. Montazeri, M. H. Shams, P. Z. Baghbadorani and N. Eskandari, *Front. Immunol.*, 2023, **14**, 1077531.
12 S. H. Jeong, H. H. Kim, S. E. Ha, M. Y. Park, P. B. Bhosale, A. Abusaliya, K. Il Park, J. D. Heo, H. W. Kim and G. S. Kim, *Int. J. Mol. Sci.*, 2022, **23**, 10965.
13 W. J. MacDonald, C. Purcell, M. Pinho-Schwermann, N. M. Stubbs, P. R. Srinivasan and W. S. El-Deiry, *Cancers*, 2025, **17**, 441.
14 D. L. Costanzo-Garvey, A. J. Case, G. F. Watson, M. Alsamraae, A. Chatterjee, R. E. Oberley-Deegan, S. Dutta, M. Y. Abdalla, T. Kielian, M. L. Lindsey and L. M. Cook, *Clin. Exp. Metastasis*, 2022, **39**, 641–659.
15 F. Zerargui, K. Saffidine, T. Guemmaz, H. Laroui, H. Trabsa, A. Baghiani, S. Khanouf and M. H. Abu Zarga, *Trop. J. Pharm. Res.*, 2023, **22**, 1417–1425.
16 R. Supino, in *Methods in Molecular Biology (Clifton, N.J.)*, ed. S. O'Hare and C. K. Atterwill, Humana Press, Totowa, NJ, 1995, vol. 43, pp. 137–149.
17 L. D. Zorova, E. A. Demchenko, G. A. Korshunova, V. N. Tashlitsky, S. D. Zorov, N. V. Andrianova, V. A. Popkov, V. A. Babenko, I. B. Pevzner, D. N. Silachev, E. Y. Plotnikov and D. B. Zorov, *Int. J. Mol. Sci.*, 2022, **23**, 482.
18 P. Pozarowski and Z. Darzynkiewicz, *Methods Mol. Biol.*, 2004, **281**, 301–311.
19 L. Schrödinger Schrödinger, *Schrödinger Release 2021-2: Ligprep*, Schrödinger Inc., New York, NY, USA, 2021.
20 L. Schrödinger Schrödinger, *Schrödinger Release 2021-2: QikProp*, Schrödinger Inc., New York, NY, USA, 2021.
21 W. Fang, J. Du, M. Nie and X. Wang, *Mol. Biol. Rep.*, 2024, **51**, 653.
22 A. Al-Aboudi, M. Abu Zarga, W. Hourani, A. Al-Rahmoni, A. Jabeen and M. I. Choudhary, *Nat. Prod. Res.*, 2025, **1–9**, 2498071.
23 B. Vue, S. Zhang and Q.-H. Chen, *Anticancer Agents Med. Chem.*, 2015, **16**, 1205–1229.
24 S. S. Yadav, J. A. Stockert, V. Hackert, K. K. Yadav and A. K. Tewari, *Urol. Oncol.:Semin. Orig. Invest.*, 2018, **36**, 349–360.
25 S. Izzo, V. Naponelli and S. Bettuzzi, *Nutrients*, 2020, **12**, 1010.
26 W. Lv, X. Sheng, T. Chen, Q. Xu and X. Xie, *J. Biomed. Biotechnol.*, 2008, **2008**, 394802.
27 M. Kłósek, D. Jaworska, G. Pietsz and E. Szliszka, *Life*, 2023, **13**, 592.
28 L. Delgado, I. Fernandes, S. González-Manzano, V. De Freitas, N. Mateus and C. Santos-Buelga, *Food Funct.*, 2014, **5**, 797–803.
29 A. Amantakul, A. Amantakul, S. Pojchamarnwiputh, N. Chattipakorn, S. C. Chattipakorn and J. Sripetchwandee, *Clin. Transl. Oncol.*, 2025, **27**, 2852–2875.
30 D. R. Green and J. C. Reed, *Science*, 1998, **281**, 1309–1312.
31 J. Chen, *Cold Spring Harbor Perspect. Med.*, 2016, **6**, a026104.
32 K. H. Vousden and C. Prives, *Cell*, 2009, **137**, 413–431.
33 B. B. Roba and A. B. Umar, *Future J. Pharm. Sci.*, 2025, **11**, 84.